Supplementary Information

for

Inhibition of the MET kinase activity and cell growth in MET-addicted cancer cells by bi-paratopic linking

Fabio Andres[1], Luisa Iamele[2], Timo Meyer[3], Jakob C. Stüber[1], Florian Kast[1], Ermanno Gherardi[2], Hartmut H. Niemann[3], Andreas Plückthun[1 *]

[1] Department of Biochemistry, University of Zurich, Winterthurerstrasse 190, 8057 Zurich, Switzerland

[2] Department of Molecular Medicine, University of Pavia, Italy

[3] Department of Chemistry, Bielefeld University, Germany

*Corresponding Author, email: plueckthun@bioc.uzh.ch

Supplementary Materials and Methods

Ribosome display selection of MET binding DARPins

After an initial low-stringency selection round with targets immobilized on multi-well plates, all subsequent panning cycles were conducted in solution using streptavidin-coated magnetic beads for the pulldown of target-DARPin complexes. As assessed by gel electrophoresis of the reverse-transcribed and PCR amplified output sequences, comparing to non-target control samples, already several of the selection pools indicated binder enrichment after the second round (Fig. S1).

In the third cycle, prior to the actual panning with the target, we applied an additional pre-panning step to the pools for MET_{741} and MET_{928} using biotinylated MET_{567} or MET_{741}, respectively. The DARPin variants binding to the epitopes present in these competitor constructs were therefore removed, directing the selection process towards the regions of the MET ectodomain which are exclusively present in the respective target construct. Gel electrophoresis after the third round of selection indicated clear enrichment in more than half of the twelve pools: MET_{567}-N2C, MET_{567}-N3C, MET_{567}-N3LC, MET_{741}-N2C, MET_{741}-N3C, MET_{928}-N2C and MET_{928}-N3C (Fig. S1b). For the fourth cycle, we applied off-rate selection to two of the pools which already showed very clear enrichment after round 2 (MET_{928}-N2C and MET_{928}-N3C). Here, the presence of a 315-fold molar excess of non-biotinylated over biotinylated target in the panning step enabled the enrichment of binder variants with slow dissociation rates (off-rates). The rest of the pools were subjected to a very stringent fourth cycle (low target concentration, several extended washing steps) without off-rate selection. After the fourth cycle, all selection pools except MET_{567}-Nr3LCr indicated strong enrichment in the gel electrophoresis analysis of the reverse-transcribed output pools (Fig. S1c and d).

After four rounds of selection we isolated and screened 95 to 190 single clones per selection pool for binding to the different target constructs by enzyme-linked immunosorbent assay (ELISA) using bacterial crude extracts. In the screening, we found specific DARPins to all of the three MET constructs used. Measuring ELISA signals at different dilutions of the crude extracts enabled the elimination of variants with poor affinities.

Sequence analysis of 4 to 26 clones per pool revealed a high fraction of unique sequences within all of the selections. We expressed and purified the unique sequences in small scale to conduct further characterization. Overall, the binding specificities seen in the initial screening could be confirmed with purified DARPins using ELISA in either a direct or a competition setup. Finally, a high percentage of variants showed binding to the desired target region to which it had been directed to in the selection process. Table ST1 summarizes the outcome of the parallel binder selections from four DARPin libraries using three target constructs.

Characterization of binders

In order to identify the subset of binders capable of binding to the endogenous MET receptor on human cells we performed flow cytometry measurements using the MET-overexpressing human gastric adenocarcinoma cell line MKN-45. We used two detection strategies to measure binding to the receptor and a competition setup to test for specificity of binding (self-competition). First, we detected DARPins after incubation on the cells using an Alexa-Fluor-488 labeled antibody binding to the N-terminal His-tag of the DARPins. Considering possible steric restrictions of the antibody binding to DARPins with epitopes close to the membrane, we also generated fusions of sfGFP to the C-terminus of all selected DARPins. The direct detection of GFP fluorescence served as a second readout in the screening in order to minimize the fraction of false negative measurements. Applying a threshold of a mean fluorescence intensity (MFI) signal three-fold higher than the signal from a non-binding DARPin (Off7) control (Off7 or Off7-sfGFP), the screening revealed 50 out of 130 binders being positive in at least one of the detection methods (Fig. S2d).

Hereafter, we analyzed a number of biophysical characteristics in order to allow for a further condensing of the binders to a diverse core set to be subjected to biological studies. We performed ELISA assays in a combinatorial competition setup to assess epitope diversity within the binder groups to the different MET ECD domains. Furthermore, we tested some of the binders for competition with the physiological MET ligand HGF/SF as well as the MET-binding bacterial invasion protein InternalinB (InlB). These binning studies revealed distinct sub-groups (bins) of binders to all of the three regions on the MET ECD (Sema/PSI, IPT1/2, IPT3/4) (Fig. S2a, b and c). We

determined dissociation rates from the full length ECD construct MET_{928} by homogeneous time-resolved fluorescence resonance energy transfer (HTRF) (Fig. S2e) to enable a relative ranking of off-rates within the epitope groups. Finally, analytical size exclusion chromatography was performed to identify and eliminate binders with unfavorable behavior in solution. We found binders of the N2C and N3C format predominantly behaving monomeric, whereas variants of the LoopDARPin design frequently showed some degree of oligomerization (Fig. S2f). These properties are probably caused by the high frequency of selected hydrophobic residues in the extended loop.

Effects of monomeric DARPins on MET-dependent cancer cells

A comprehensive analysis of a large number of MET-binding DARPins allowed the selection of a smaller set of binders with diverse binding characteristics. Aiming at the development of engineered binding proteins targeting MET on cancer cells, where the mechanism of action might involve interfering with ligand-dependent or ligand-independent receptor activation, we performed a first assessment of biological effects of single, monomeric DARPins on the two MET-amplified and gastric carcinoma cell lines KATOII and SNU-5, which were shown to be dependent on signaling via MET for proliferation and survival. We used the XTT proliferation assay, a readout for the reductive potential of mitochondrial enzymes as a measure for cellular proliferation. KATOII and SNU-5 cells partially respond to the single-chain Fv fragment 5D5, the precursor antibody of onartuzumab. ScFv-5D5 was tested up to a concentration of 150 nM in a five-day treatment, where it inhibits cell proliferation measured by XTT by about 20% on KATOII and by about 50% on SNU-5 cells. Both cell lines furthermore respond to the selective tyrosine kinase inhibitors (TKIs) SU11274 and PHA-665752 by complete growth inhibition and presumably apoptosis at concentrations from about 1 μM or 100 nM, respectively (Fig. S4b and c). On the other hand, both cell lines do not show significant inhibition of proliferation when incubated with 0.5 μM of single DARPins for five days (Fig. S4a). We conclude from these findings that binding of monovalent DARPins with diverse specificities to the MET receptor is not sufficient to induce any effect that is translated into altered growth behavior of the two MET-addicted cell lines. Therefore, we focused on studying the activities of bivalent and bispecific binding molecules to the MET ECD, which have the potential for enforcing

conformational changes and/or restrictions to the receptor by either intra- or intermolecular crosslinking of its extracellular domains.

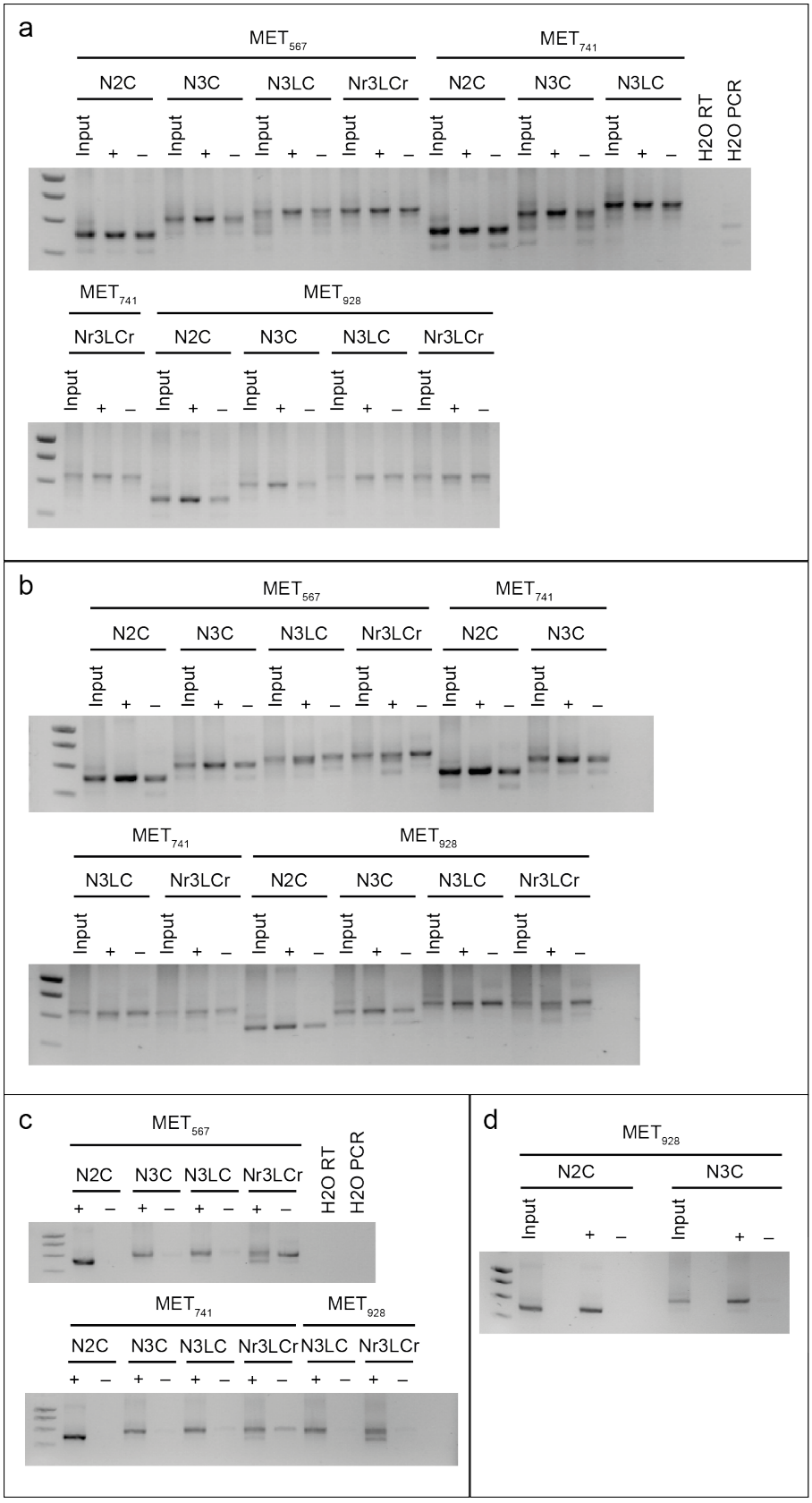

Supplementary Fig. S1. Agarose gel electrophoresis of reverse-transcribed and PCR-amplified sequence pools after ribosome display selection cycles. Selected sequence pools after target panning (+) are compared to control panning reactions without target (–). Reverse-transcribed and amplified input RNA is shown as control. Panels depict selected pools after the second (a), third (b) and fourth panning round (c). The two selection pools depicted in (d) are derived from a fourth round with off-rate selection.

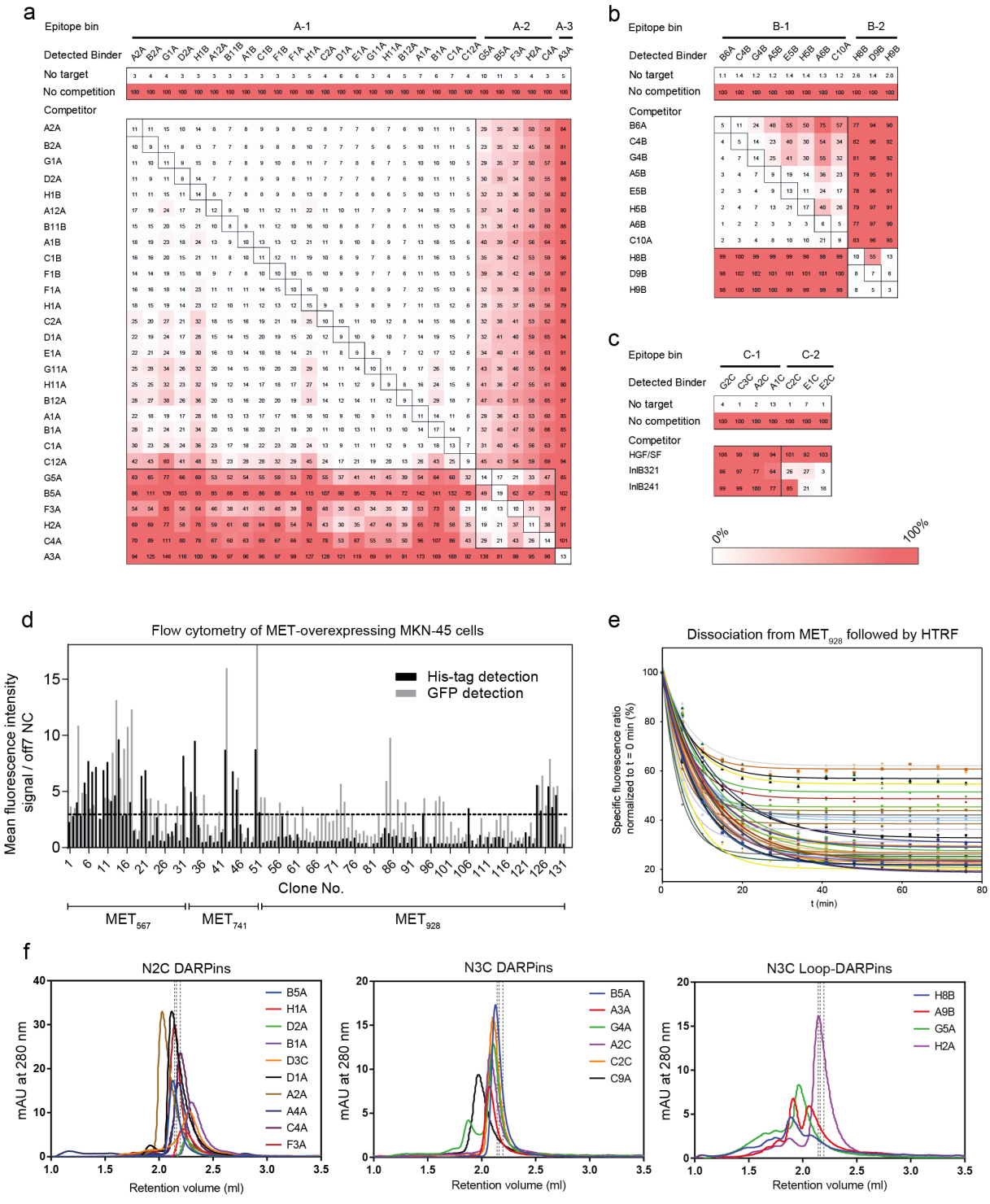

Supplementary Fig. S2. Characterization of selected MET binding DARPins. (a-c) Epitope binning analysis by ELISA within different binder groups; (d) flow cytometry screening for cell binding on MKN-45 cells; (e) dissociation measurement by HTRF assay for off-rate ranking; (f) analytical size exclusion chromatography. DARPins of different formats are shown in separate panels. Dashed lines depict the calculated expected elution volume for an average DARPin of the N3C Loop, N3C or N2C format, from left to right.

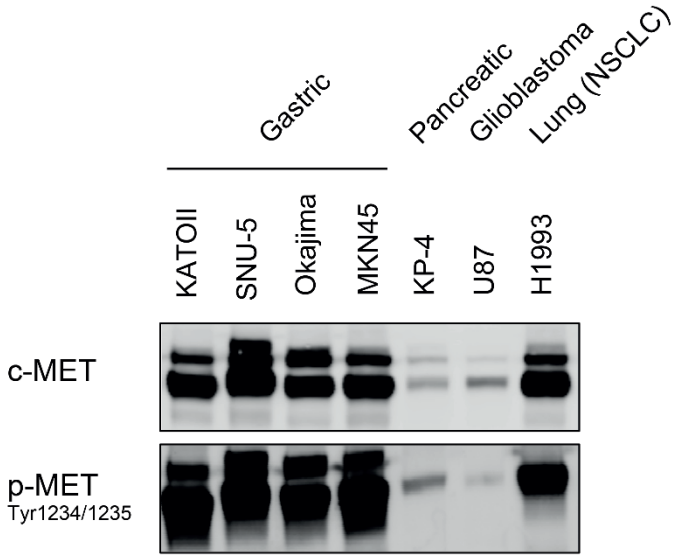

Supplementary Fig. S3. Immunoblotting of MET and p-MET (Y1234/1235) in a panel of cell lines of different origin.

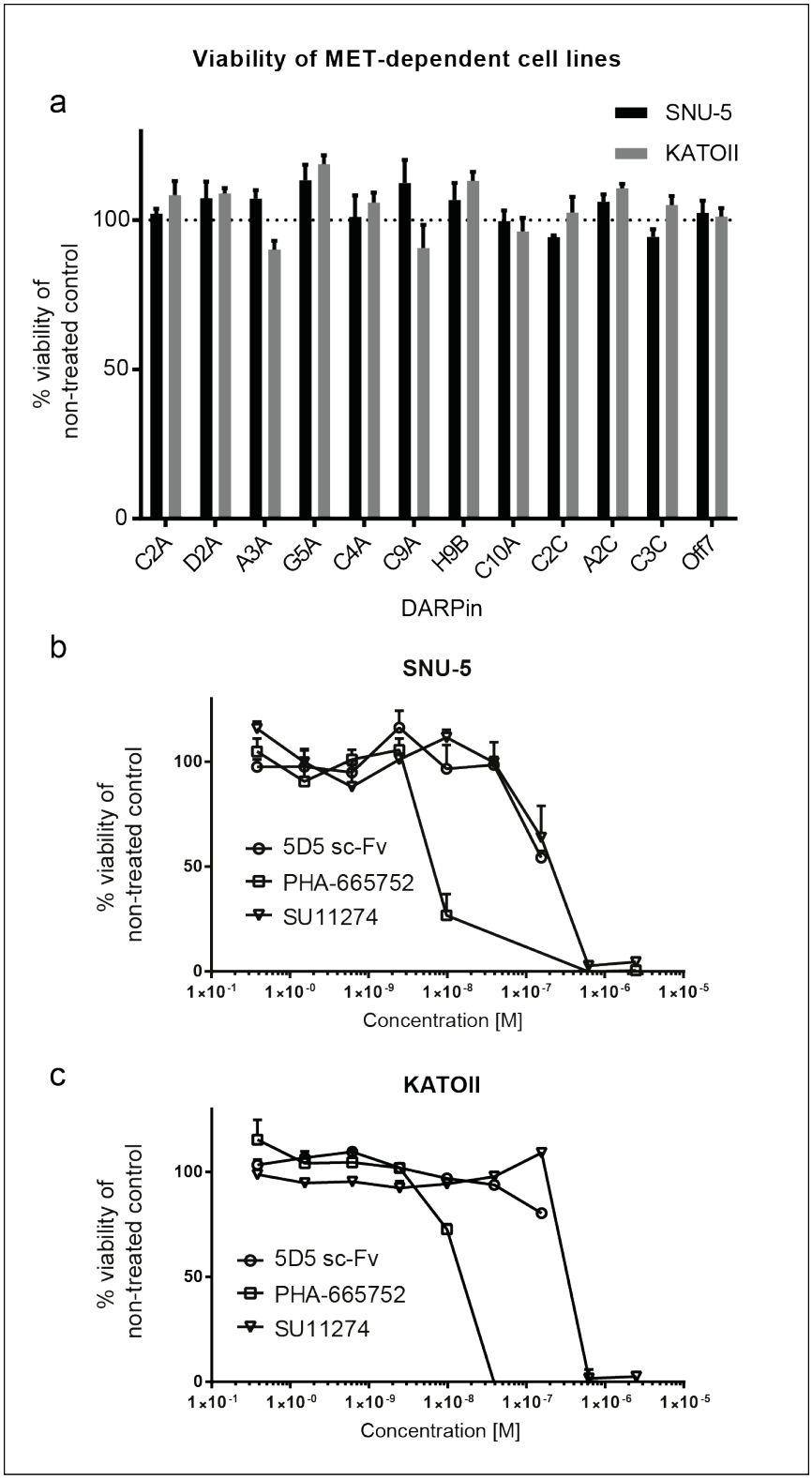

Supplementary Fig. S4. Proliferation assay with two MET-dependent gastric carcinoma cell lines treated with monomeric DARPins, scFv 5D5 or MET-TKIs. (a) Bars represent means of triplicate measurements with standard deviations of cells treated with 0.5 μM monomeric MET-DARPins and a control DARPin off7. (b and c) Cells were treated with titrations of anti-MET scFv 5D5 or MET TKIs and proliferation signals plotted as means of triplicates with standard deviations. Treatment was performed for 4 days and all plotted signals were normalized to PBS-treated control.

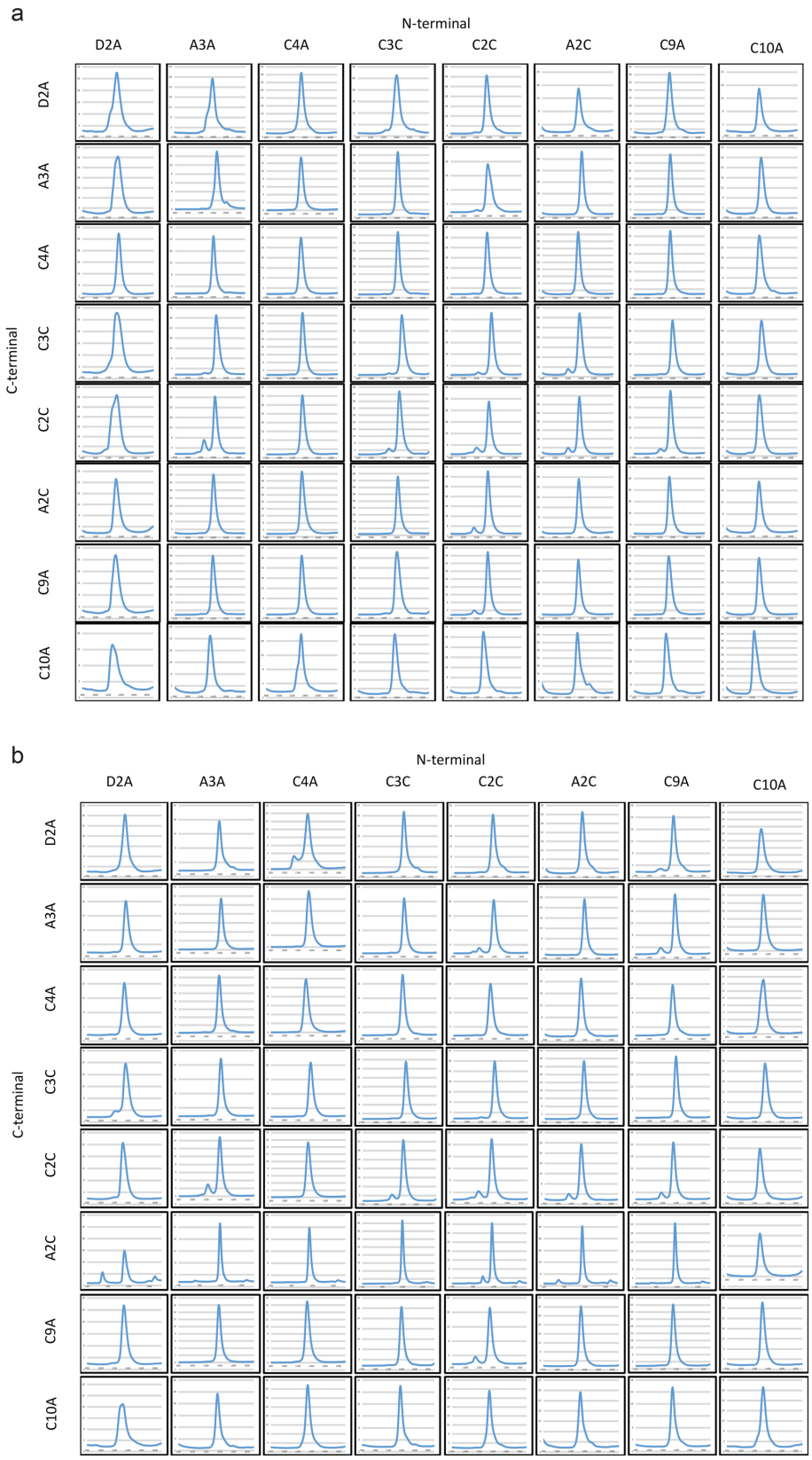

Supplementary Fig. S5. Analytical Size Exclusion Chromatography of 128 bispecific DARPin-DARPin fusions after purification by HisPur™ Cobalt resin (IMAC) in 96-well format, Triton-X114 wash for endotoxin removal, buffer exchange and sterile filtration. A Superdex-200 GL 5/150 column was used on an Agilent HPLC system using PBS as running buffer and a flow rate of 0.2 ml/min. Elution profiles are shown for bi-paratopic DARPins with a short linker (L1, 5 amino acids) in panel a, and for DARPins with a long linker (L2, 20 amino acids) in panel b.

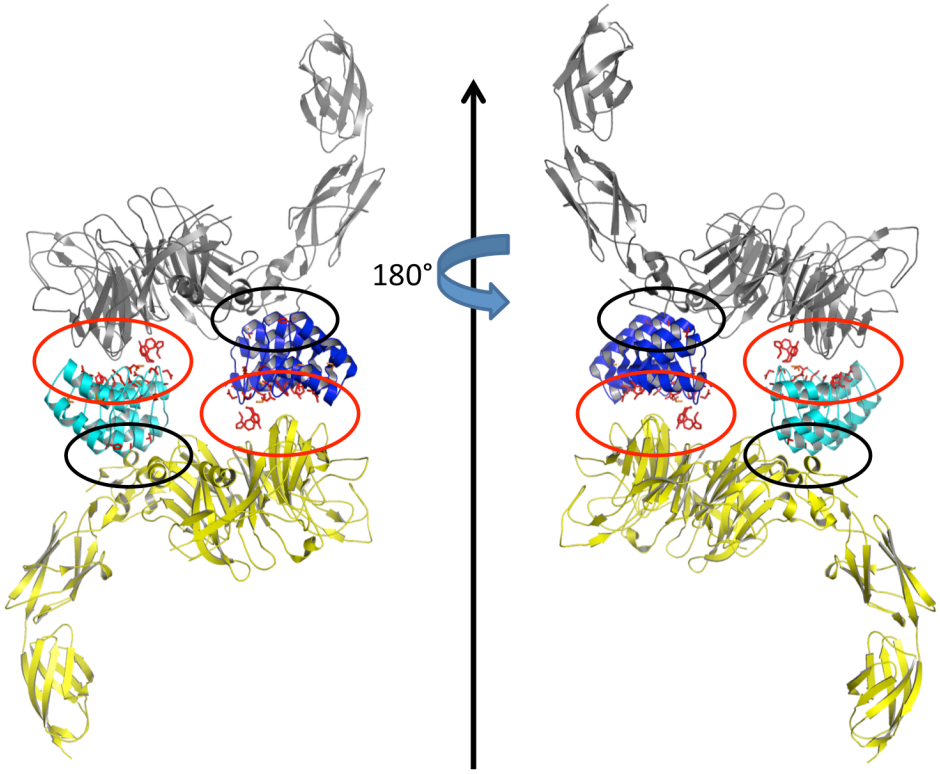

Supplementary Fig. S6. Contacts between the DARPin A3A and MET in the crystal lattice.
One MET molecule makes contacts with two DARPins and each DARPin contacts two MET molecules. Randomized residues of A3A are shown as red sticks. A3A residues mutated during the selection are shown as orange sticks. One DARPin / MET contact is mostly mediated by randomized DARPin residues and involves the MET Sema domain (red oval; interface 1). This interface is larger (~760 Å^2). We consider it to be the physiological contact between A3A and MET. We made this assembly part of the asymmetric unit. Thus, in our choice of the asymmetric unit, the dark blue DARPin binds the yellow MET molecule and the cyan DARPin binds the gray MET molecule.
The other DARPin / MET contact is mostly mediated via conserved residues of the DARPin scaffold and involves the MET Sema + PSI domains (black oval, interface 2). This interface is significantly smaller (~510 Å^2). We consider it to be a crystal packing contact. Thus, in our choice of the asymmetric unit, the contact between the blue DARPin and the gray MET molecule and the contact between the cyan DARPin and the yellow MET molecule are contacts between molecules of different, symmetry-related asymmetric units.

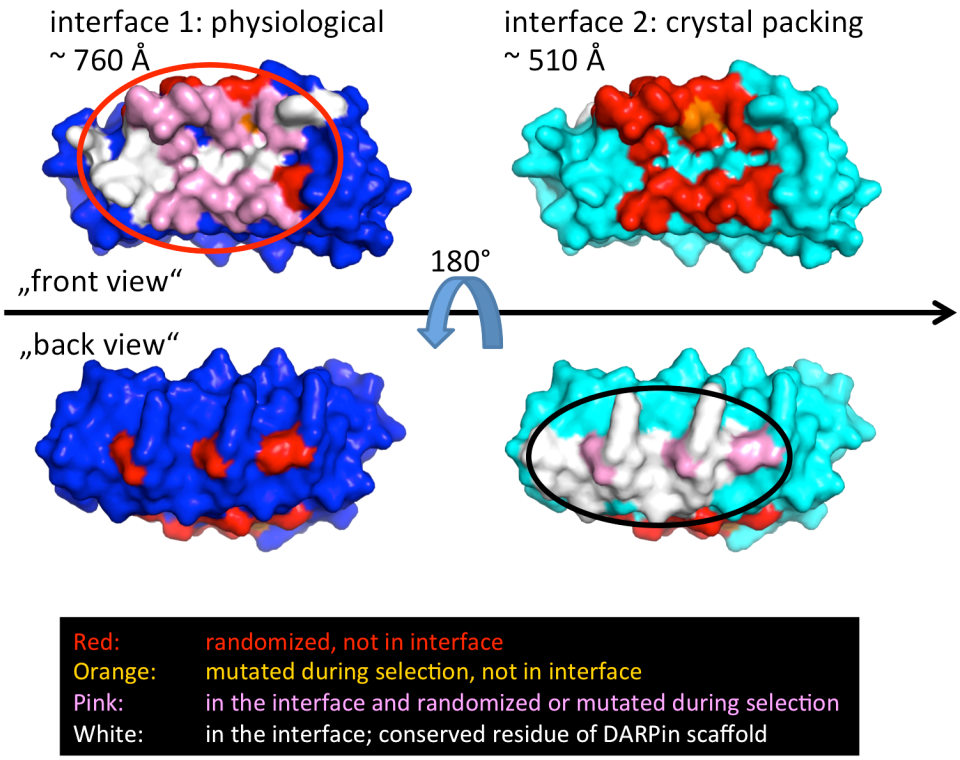

Supplementary Fig. S7. DARPin residues that contact MET are color-coded according to their conservation. The interfaces are highlighted by a red or black oval as in Supplementary Fig. S6. DARPins are colored as those DARPins contacting the yellow MET molecule in Supplementary Fig. S6. The DARPin that we consider to form the biologically relevant contact with MET is shown in blue. The DARPin that we consider to form a crystal packing contact with MET is shown in cyan. Both DARPins are shown in the same orientation above or below the arrow. The bottom views („back view“) are rotated by 180° around a horizontal axis with respect to the top views („front view“).
Residues that contact MET are shown in white or pink.
Residues in white belong to the conserved DARPin scaffold.
Residues in pink are randomized residues or residues that were mutated during selection.
Residues that do not contact MET are shown in blue, cyan, red or orange.
Residues in blue or cyan belong to the conserved scaffold and are not part of the interface.
Residues in red were randomized and are not part of the interface.
Residues in orange were mutated during selection and are not part of the interface.

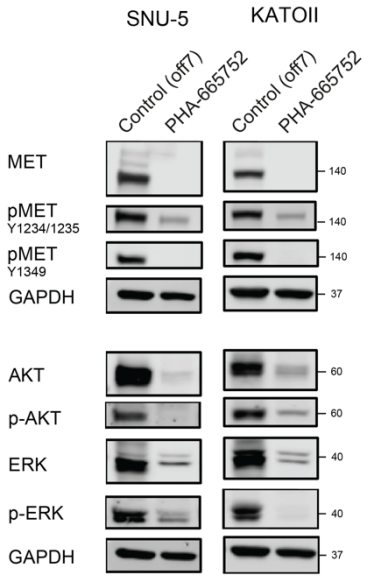

Supplementary Fig. S8. The MET-selective tyrosine kinase inhibitor PHA-665752 dramatically decreases levels of MET receptor, Akt and Erk1/2 in *MET*-amplified gastric carcinoma cells SNU-5 and KATOII. Whole-cell lysates were adjusted to equal concentrations of total protein, separated by SDS-PAGE and transferred to blotting membranes. Proteins and phosphorylation status were detected by specific primary antibodies, followed by fluorescently labeled secondary antibodies. Signals were recorded on a fluorescence scanner. GAPDH was detected as a loading control.

a

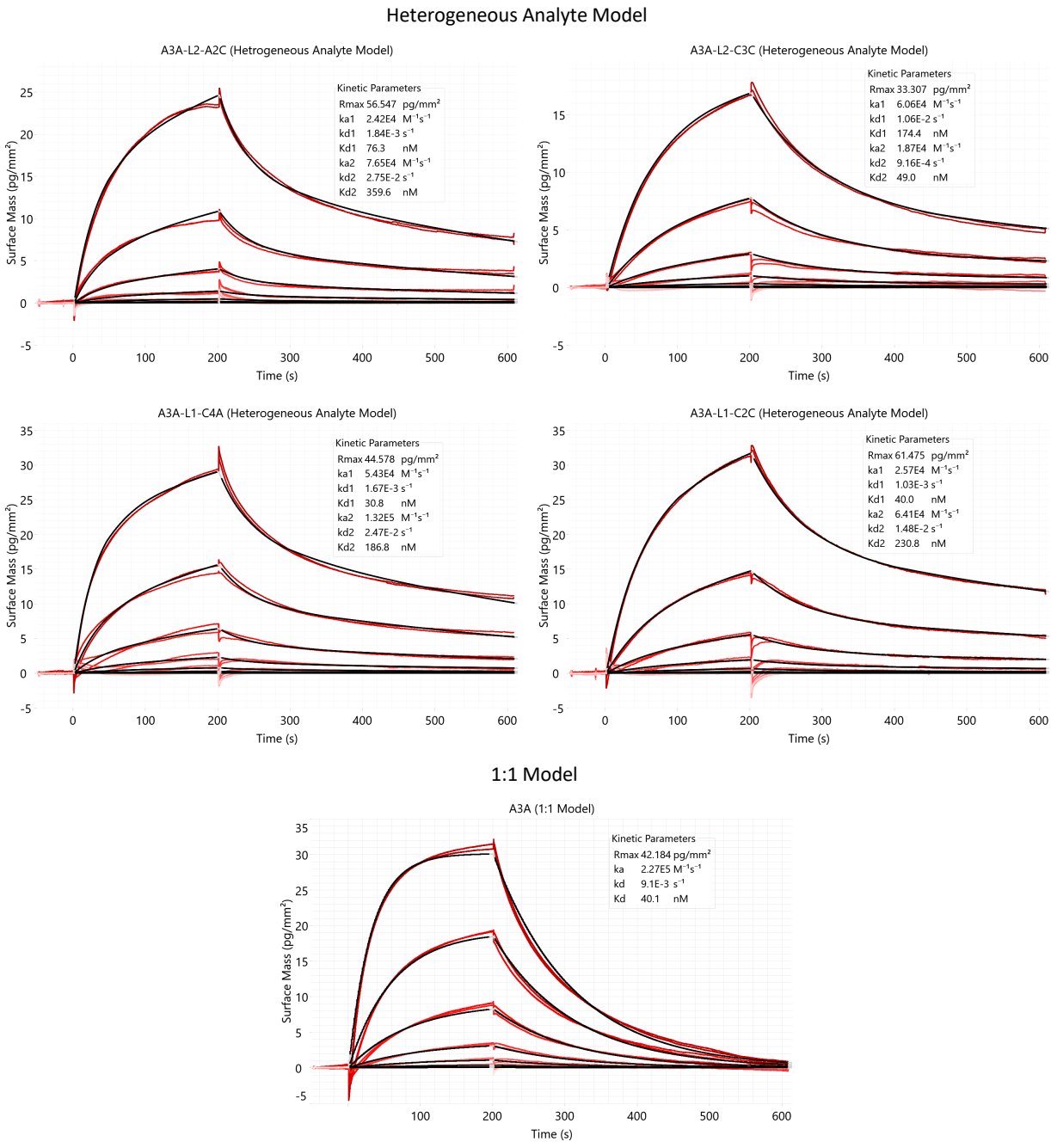

b Summary of SPR kinetic binding data for monovalent and bi-paratopic DARPins from (**a**).

	$k_{on,1}$ [M^{-1} s^{-1}]	$k_{on,2}$ [M^{-1} s^{-1}]	$k_{off,1}$ [s^{-1}]	$k_{off,2}$ [s^{-1}]	$K_{D,1}$ [nM]	$K_{D,2}$ [nM]
A3A	$22.7 \cdot 10^4$		$9.10 \cdot 10^{-3}$		40	
A3A-L2-A2C	$2.42 \cdot 10^4$	$7.65 \cdot 10^4$	$1.84 \cdot 10^{-3}$	$27.5 \cdot 10^{-3}$	76	360
A3A-L2-C3C	$1.87 \cdot 10^4$	$6.06 \cdot 10^4$	$0.92 \cdot 10^{-3}$	$10.6 \cdot 10^{-3}$	49	174
A3A-L1-C4A	$5.43 \cdot 10^4$	$13.2 \cdot 10^4$	$1.67 \cdot 10^{-3}$	$24.7 \cdot 10^{-3}$	31	187
A3A-L1-C2C	$2.57 \cdot 10^4$	$6.41 \cdot 10^4$	$1.03 \cdot 10^{-3}$	$14.8 \cdot 10^{-3}$	40	231

c

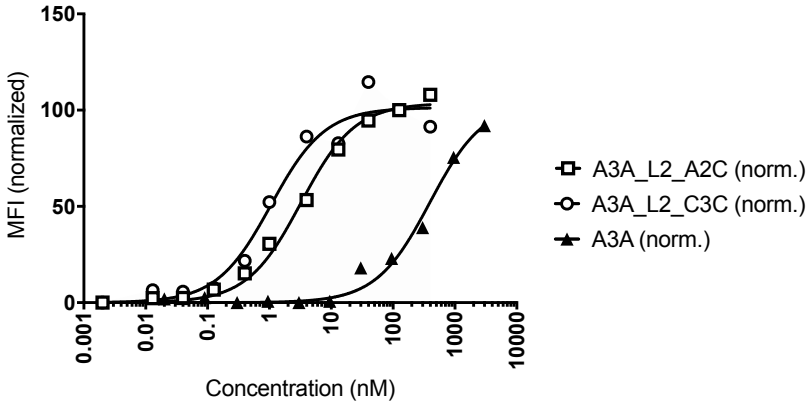

Supplementary Figure S9. Test of intramolecular vs. intermolecular binding of bi-paratopic DARPins. (a) GCI (grating-coupled interferometry, Creoptix WAVE system) binding curves of different bi-paratopic DARPins, all containing DARPin A3A, and the monovalent DARPin A3A are shown in comparison. As expected, only for the monovalent binder A3A (bottom), the 1:1 Langmuir model adequately fits the data, for the bi-paratopic binders these attempted 1:1 fits are not shown. From fitting the bi-paratopic binders with a heterogeneous analyte model, it can be seen that no slower off-rates are observed than for the monovalent binder, thus excluding that bivalent binding is intramolecular. Even at the high density of MET immobilized on the chip, shown here, a neighboring MET molecule can apparently not be reached. (b) The determined binding data are consistent with the two constituting DARPins binding alternatively, but not bivalently, as now slower off-rate is observed. (c) Flow cytometry titration of two bi-paratopic DARPins from (a) vs. the monovalent binder A3A on KATOII cells. Normalized mean fluorescent intensities are shown. The avidity gain of the bi-paratopic binders on cells is clearly seen, indicating that the avidity gain on cells is intermolecular.

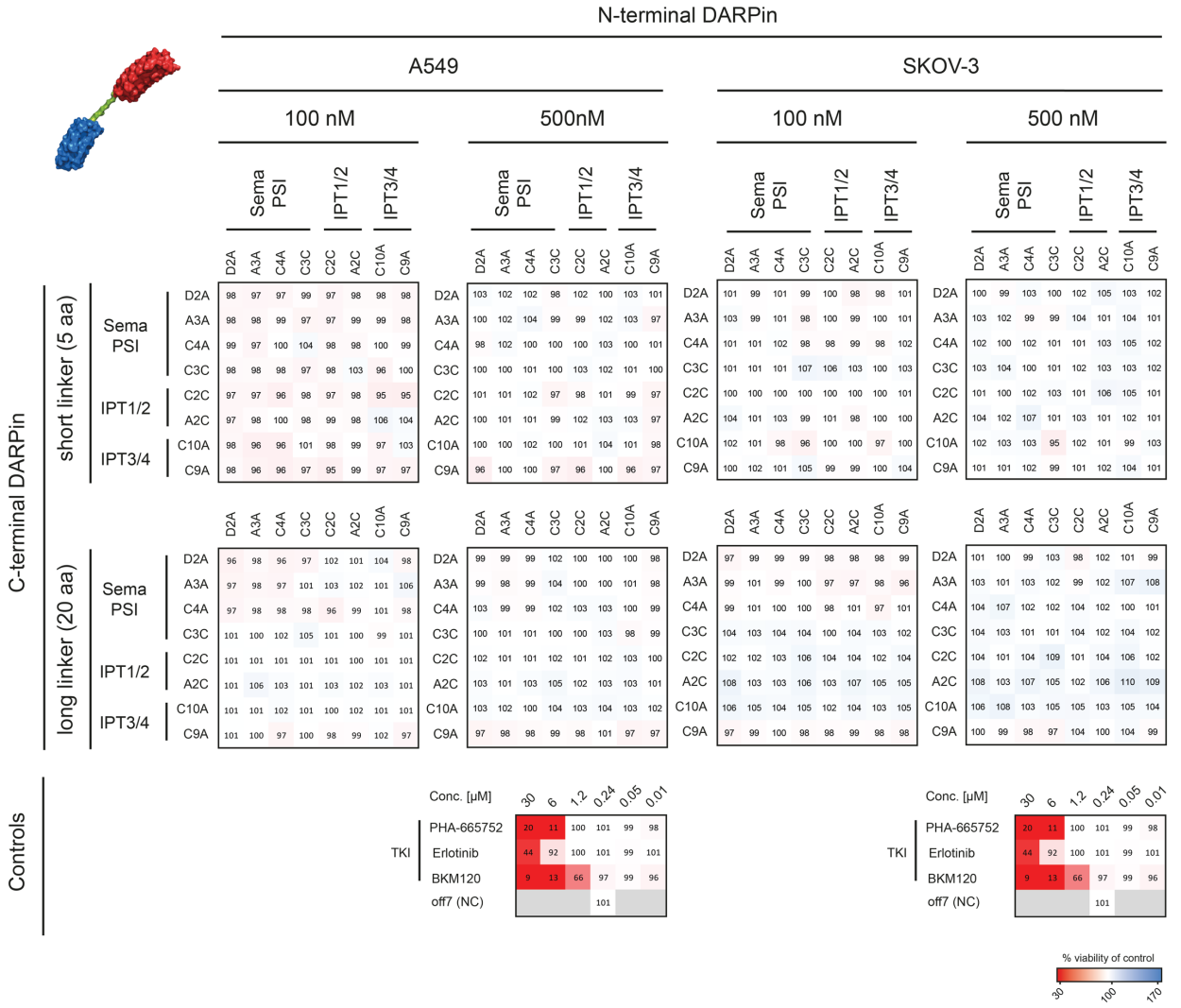

Supplementary Fig. S10. Bi-paratopic DARPins induce no anti- or pro-proliferative effects on HGF-sensitive cell lines A549 and SKOV-3 not having *MET*-amplification. The combinatorial screening for changes in cell proliferation by XTT assays is shown in a heatmap representation obtained from triplicate proliferation measurements and calculated as a percentage of non-treated controls. The resulting patterns are shown for A549 cells on the left and for SKOV-3 cells on the right. The top panels correspond to the treatment with DARPin-DARPin fusion constructs carrying a short linker (5 amino acids), lower panels show the corresponding data for the constructs with a long linker (20 amino acids). Each grid of molecules was tested at a final concentration of 100 nM (left) and 500 nM (right). Controls for selective tyrosine kinase inhibitors (TKI), the PI3 Kinase inhibitor BKM120 and the MBP-binding control DARPin Off7 are shown at the bottom. The color scheme was set to a range from 30% (red) to 170% (blue) relative proliferation, with white indicating no change in proliferation compared to the control.

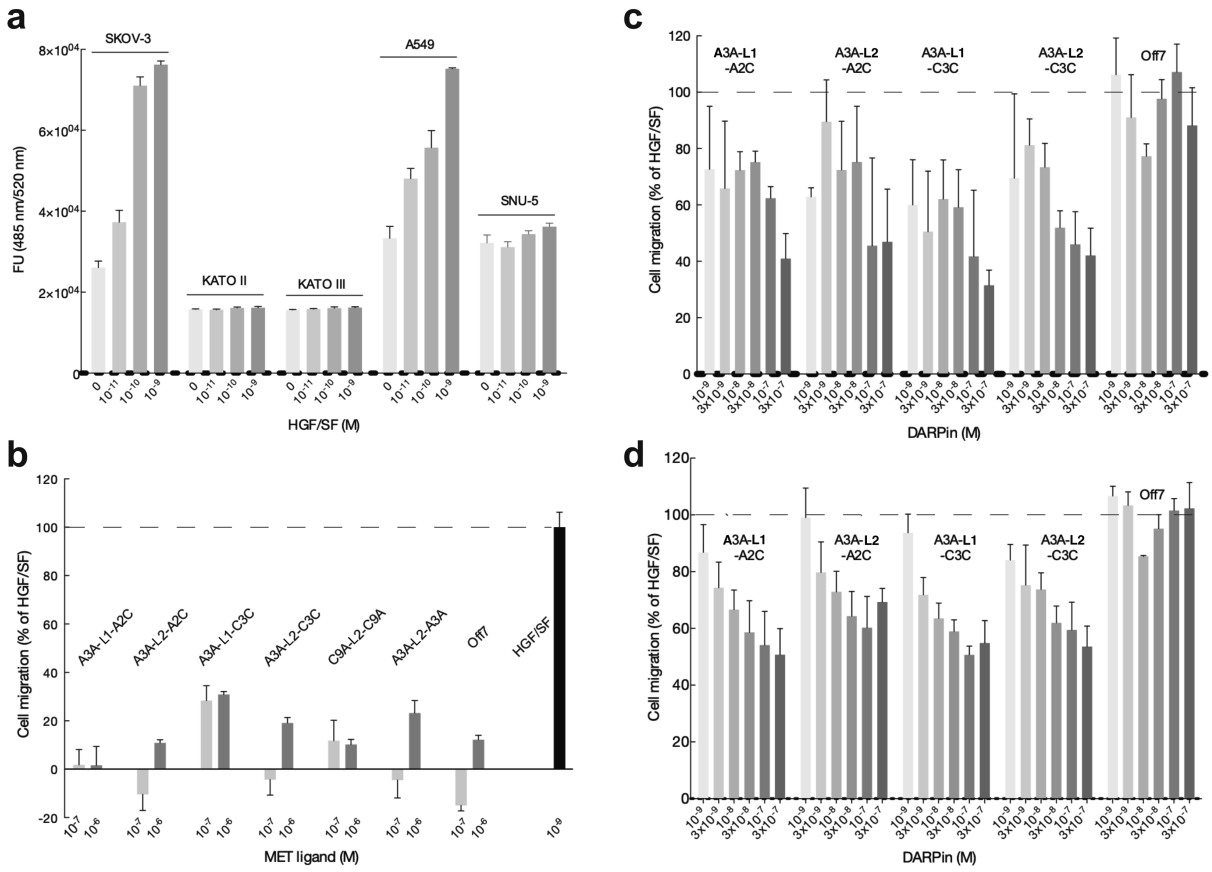

Supplementary Fig. S11. Motility assays. (a) Motility response of the lung carcinoma line A549, the ovarian carcinoma line SKOV-3 and the gastric carcinoma lines KATOII, KATOIII and SNU-5 to HGF/SF. No response is seen in the gastric carcinoma lines with amplified *MET* locus and constitutively active MET, in contrast to the strong response observed in A549 and SKOV-3 cells. (b) Agonistic activity of the anti-MET DARPins in motility assays in in A549 cells. Note that the agonistic activities are very weak, as the DARPins are used at 1,000 to 10,000-fold higher concentrations than HGF/SF, still displaying only 20-25 % of the activity. Most of the DARPins lack agonistic activity. (c, d) Antagonistic activity of selected DARPins on HGF/SF-induced motility of A549 (c) and SKOV-3 (d) cells.

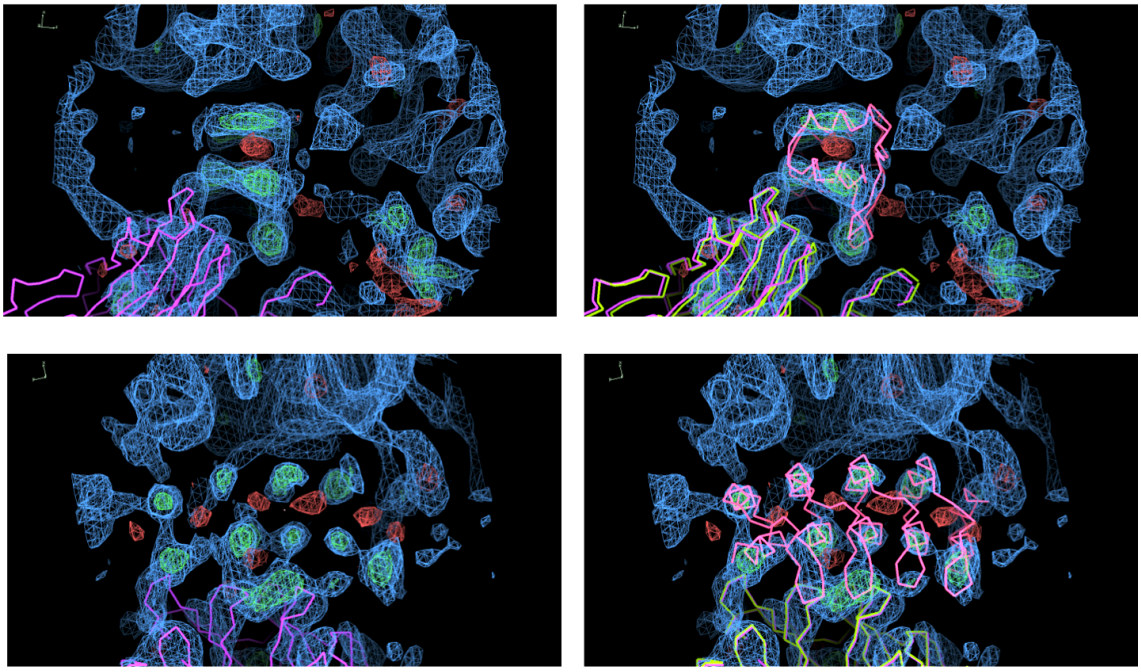

Supplementary Fig. S12. Unbiased electron density for the DARPin after molecular replacement and rigid body refinement with only MET and InlB.
Two MET/InlB complexes from PDB ID 2UZY were located with Phaser. The Sema domains were replaced by the Sema domain of PDB ID 1SHY and PSI, IPT1 and IPT2 were replaced by those of PDB ID 5LSP. Rigid body refinement was performed with ten rigid bodies, one for each domain (two times each: Sema, PSI, IPT1, IPT2, InlB) in conjunction with grouped B-factor refinement.
The resulting model without DARPin had R_{work} = 34.45% and R_{free} = 36.22% and was used to calculate unbiased electron density that is shown in the region of the DARPin above. The same density is shown without the DARPin (left) and overlaid with the DARPin taken from the deposited structure (right). 2Fo-Fc density contoured at 1.5 σ is shown in blue, Fo-Fc density is shown in green at +3 σ and in red at -3σ.

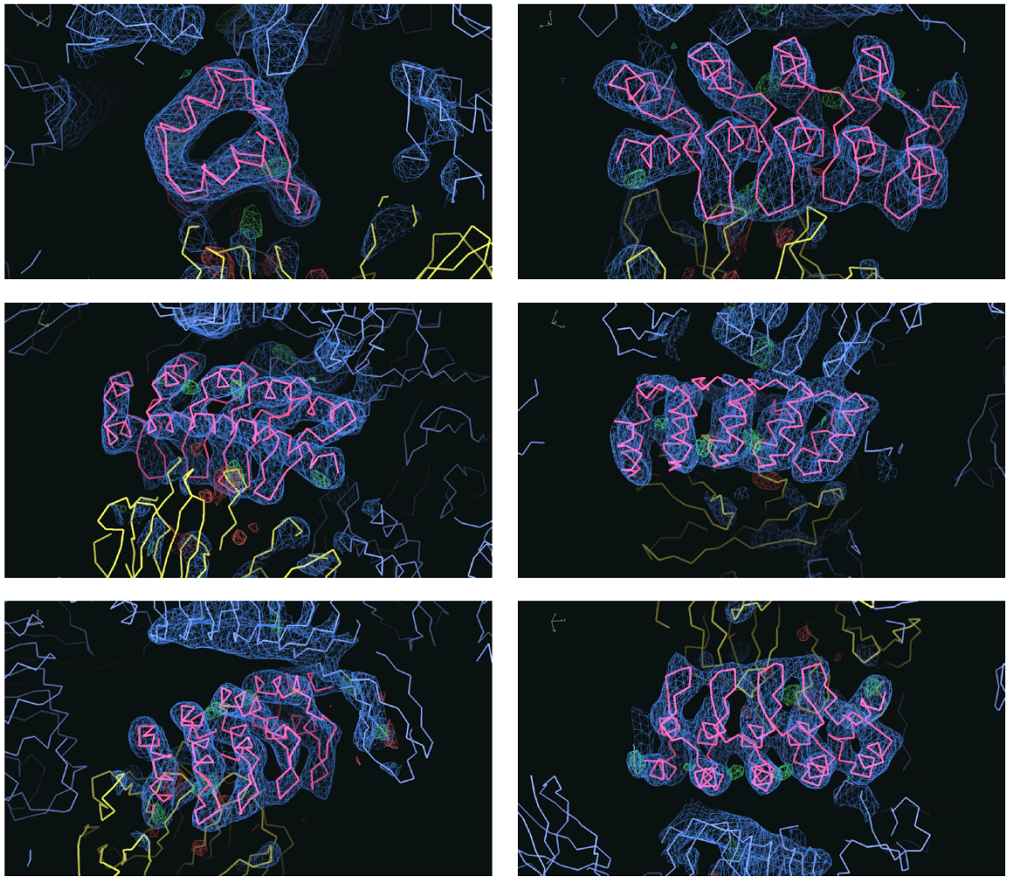

Supplementary Fig. S13. DARPin electron density of the final structure. The 2Fo-Fc electron density map at 6 Å resolution and contoured at 1.3 σ clearly shows that the position and orientation of DARPin A3A (pink) is well defined within the structure of the A3A/MET_{741}/$InlB_{321}$-complex. The randomized residues of the DARPin contact the MET_{741} Sema domain (yellow).

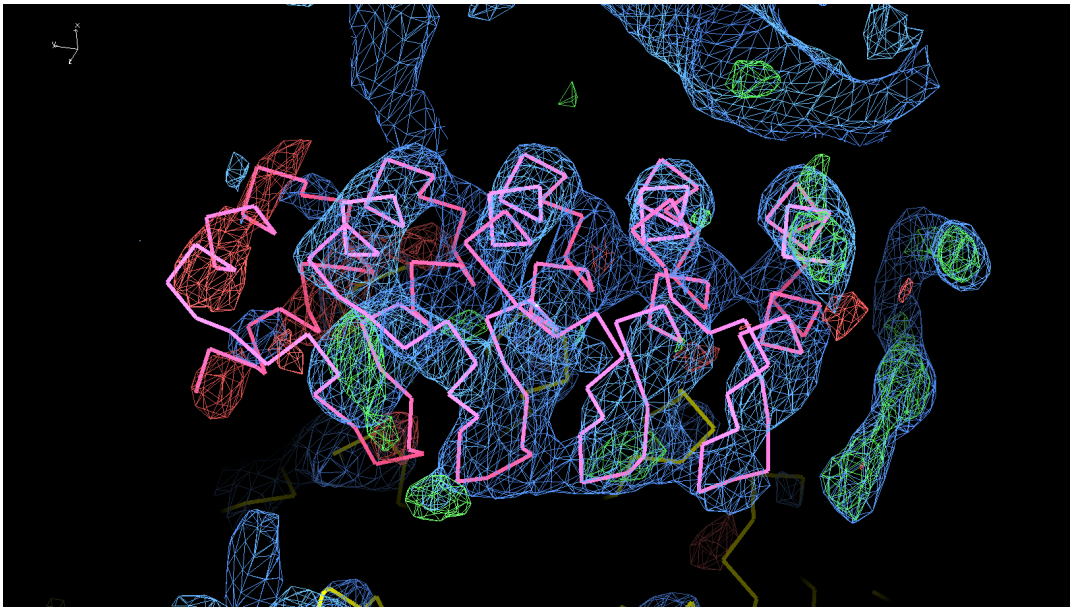

Supplementary Fig. S14. Verification of the DARPin register.
One DARPin (chain C) was shifted by one repeat unit towards its N-terminus (ID „B“ in Supplementary Table ST4). Five rounds of rigid body refinement were calculated with phenix.refine. The resulting 2Fo-Fc electron density contoured at 1.5 σ is shown in blue and the resulting Fo-Fc difference density is shown in green at +3 σ and in red at -3 σ. The shift towards the N-terminus corresponds to a shift to the left in the view shown above. It is apparent that, after shifting the DARPin from its original position, the N-terminal capping repeat is out of density, while there is clear positive difference density in the region where the C-terminal capping repeat was originally placed.

Supplementary Table ST1. Statistics of initial single clone analysis after ribosome display binder selection

Target	MET_{567}				MET_{741}				MET_{928}			
DARPin Library	N2C	N3C	N3LC	Nr3LCr	N2C	N3C	N3LC	Nr3LCr	N2C	N3C	N3LC	Nr3LCr
# of clones screened	95	95	95	95	190	190	190	190	190	190	190	190
% ELISA positive signals[1]	21%	4%	10%	5%	19%	21%	29%	20%	83%	87%	50%	82%
% positives with desired target specificity[2]	100%	100%	100%	100%	86%	63%	73%	75%	70% [3]	70% [3]	70% [3]	70% [3]
# of clones sequenced	20	4	8	4	12	3	5	9	24	28	19	26
# of unique sequences	16	3	7	3	8	3	4	4	22	22	16	22

[1] positive signal considered as > 3-fold higher than non-target control
[2] no signal / no competition with respective shorter target construct
[3] value derived from smaller subset at a later screening

Supplementary Table ST2. Kinetic binding data for MET binding DARPins determined by SPR.

Target	MET_{567}				MET_{741}				MET_{928}			
DARPin	k_{on} [M^{-1} s^{-1}]	k_{off} [s^{-1}]	K_D [M]	R_{max} [RU]	k_{on} [M^{-1} s^{-1}]	k_{off} [s^{-1}]	K_D [M]	R_{max} [RU]	k_{on} [M^{-1} s^{-1}]	k_{off} [s^{-1}]	K_D [M]	R_{max} [RU]
D2A (Sema)	6.76×10^{5}	4.78×10^{-3}	7.07×10^{-9}	50.2	8.34×10^{5}	3.18×10^{-3}	3.81×10^{-9}	42.8	5.73×10^{5}	4.32×10^{-3}	7.54×10^{-9}	27.4
C3C (Sema)	7.80×10^{5}	2.60×10^{-2}	3.33×10^{-8}	64.4	8.36×10^{5}	2.44×10^{-2}	2.92×10^{-8}	84.3	1.13×10^{6}	2.35×10^{-2}	2.08×10^{-8}	45.4
C4A (Sema)	1.18×10^{6}	1.30×10^{-2}	1.09×10^{-8}	61.5	*	*	1.06×10^{-8}	76.1	*	*	2.07×10^{-8}	38.7
A3A (Sema)	3.86×10^{5}	9.13×10^{-3}	2.36×10^{-8}	135.8	4.31×10^{5}	1.01×10^{-2}	2.35×10^{-8}	94.8	3.72×10^{5}	1.52×10^{-2}	4.08×10^{-8}	57.6
G5A (Sema)	4.00×10^{4}	5.93×10^{-3}	1.48×10^{-7}	36.3	5.15×10^{4}	2.35×10^{-3}	4.57×10^{-8}	54.9	9.17×10^{4}	3.29×10^{-3}	3.59×10^{-8}	24.6
C2C (IPT1/2)	*	*	1.80×10^{-7}	27.8	*	*	1.05×10^{-7}	60.1	*	*	1.84×10^{-8}	25.2
A2C (IPT1/2)	no binding				4.82×10^{5}	1.04×10^{-2}	2.15×10^{-8}	23.6	*	*	1.84×10^{-8}	14.2
C9A (IPT3/4)**					no binding				1.84×10^{6}	1.28×10^{-3}	6.99×10^{-10}	48.2
C10A (IPT3/4)**									2.11×10^{5}	1.51×10^{-4}	7.17×10^{-10}	54.4
A9B (IPT3/4)**									4.22×10^{4}	2.56×10^{-4}	6.06×10^{-9}	43.0
H8B (IPT3/4)**									8.00×10^{4}	1.94×10^{-4}	2.42×10^{-9}	18.4

* equilibrium binding model used

** kinetic titration model used

Binding and dissociation of DARPins to immobilized MET targets was recorded at 5 concentrations between 0.6 and 300 nM. Unless indicated by asterisks, on- and off-rates were determined by fitting to a kinetic Langmuir model. In cases of poor quality of kinetic fitting we used an equilibrium binding model to assess the K_D as the concentration of DARPin at half saturation of the epitopes (*). In cases of slower and therefore incomplete dissociation prior to the injection of the next concentration, we used a kinetic titration model (Karlsson *et al,* 2006).

Supplementary Table ST3. Crystallographic data collection and refinement statistics.

Data collection statistics	
Beam line	DESY P13
Wavelength	0.97720
Space group	$P3_1$
Unit cell dimensions (Å), (°)	a = b = 144.87
	c = 128.90
	α = β = 90
	γ = 120
Resolution (highest resolution shell) (Å)	48.15 – 6.00 (6.70 – 6.00)
Completeness (%)	99.9 (100.0)
Multiplicity	7.4 (7.7)
Observations	56550 (16734)
Unique reflections	7600 (2174)
I/σ(I)	5.2 (1.4)
R_{merge} (%)	27.5 (170.1)
R_{meas} (%)	29.6 (182.2)
R_{pim} (%)	10.7 (64.6)
CC(1/2)	98.2 (55.2)
Molecules per asymmetric unit	2
Solvent content (%)	58.45
Wilson B-factor (A²)	424
Refinement statistics	
Resolution (highest resolution shell) (Å)	48.15 – 6.00 (7.55 – 6.00)
R_{work} (%)	26.25 (32.69)
R_{free} (%)	27.09 (34.49)
Average B-factor (A²)	317

Supplementary Table ST4: Verification of the DARPin register

ID	Shift	1. RBR		2. RBR		3. RBR		4. RBR		5. RBR	
		R_{work} (%)	R_{free} (%)	R_{work} (%)	R_{free} (%)	R_{work} (%)	R_{free} (%)	R_{work} (%)	R_{free} (%)	R_{work} (%)	R_{free} (%)
A	**Chain C C-terminal**	28.53	30.72	28.58	30.80	28.67	30.93	28.57	30.91	28.62	30.63
B	**Chain C N-terminal**	28.43	30.65	28.46	30.11	28.41	30.40	28.30	30.26	28.38	30.64
C	**Chain F C-terminal**	28.20	29.07	28.23	29.37	28.24	29.54	28.21	29.31	28.35	29.19
D	**Chain F N-terminal**	29.14	28.86	29.36	29.43	29.28	29.24	29.20	28.83	29.27	29.52
E	**Chain C+F C-terminal**	30.04	31.85	30.28	32.11	30.42	31.88	30.67	31.83	30.67	31.89
F	**Chain C C-terminal + Chain F N-terminal**	30.41	31.40	30.60	31.74	30.65	31.45	30.60	31.62	30.63	31.76
G	**Chain C N-terminal + Chain F C-terminal**	30.00	32.43	30.12	32.49	30.22	32.54	30.19	32.56	30.20	32.22
H	**Chain C N-terminal + Chain F N-terminal**	31.65	32.63	31.89	33.07	32.09	32.71	31.95	33.04	31.88	32.98
I	**Deposited Structure**	26.49	27.40	26.55	27.41	26.65	27.56	26.63	27.55	26.54	27.42

One or both DARPins (chains C and F) were intentionally shifted by one repeat unit to the N- or C-terminus. Then, five iterations of rigid body refinement (RBR) were calculated with phenix.refine. The resulting R_{work} and Rf_{ree} values are tabulated. For comparison and as a reference, we performed five iterations of RBR with the deposited structure (ID "I").